Photonic bandgap Bragg fiber sensors for bending/displacement detection

Hang Qu,[1] Tiberius Brastaviceanu,[2] Francois Bergeron,[2] Jonathan Olesik,[2] Ivan Pavlov,[2] Takaaki Ishigure,[3] and Maksim Skorobogatiy[1,*]

[1]Genie Physique, Ecole Polytechnique de Montreal, C. P. 6079. Succ. Centre-ville, Montreal, Quebec H3C 3A7, Canada

[2]Tactus Scientific Inc, Campus des Technologies de la Sante, 5795 de Gaspe, Montreal, Quebec H2S 2X3, Canada

[3]Department of Applied Physics and Physico Informatics, Keio University, Kohoku Ku, Yokohama, Japan

*Corresponding author: maksim.skorobogatiy@polymtl.ca

Received 23 May 2013; revised 31 July 2013; accepted 5 August 2013;
posted 6 August 2013 (Doc. ID 191090); published 29 August 2013

We demonstrate an amplitude-based bending/displacement sensor that uses a plastic photonic bandgap Bragg fiber with one end coated with a silver layer. The reflection intensity of the Bragg fiber is characterized in response to different displacements (or bending curvatures). We note that the Bragg reflector of the fiber acts as an efficient mode stripper for the wavelengths near the edge of the fiber bandgap, which makes the sensor extremely sensitive to bending or displacements at these wavelengths. Besides, by comparison of the Bragg fiber sensor to a sensor based on a standard multimode fiber with similar outer diameter and length, we find that the Bragg fiber sensor is more sensitive to bending due to the presence of a mode stripper in the form of a multilayer reflector. Experimental results show that the minimum detection limit of the Bragg fiber sensor can be as small as 3 μm for displacement sensing.

OCIS codes: (060.2370) Fiber optics sensors; (060.5295) Photonic crystal fibers; (060.4005) Microstructured fibers.

http://dx.doi.org/10.1364/AO.52.006344

1. Introduction

Fiber-optic bending/displacement sensors have been extensively used in various scientific and industrial fields. Recently, several research groups have demonstrated using optical-fiber bending sensors for bio- and medical sensing applications. For example, the SENSORICA group [1] has used their fiber bending sensors to detect the contraction of a small bundle of cardiac muscle cells. Mitachi *et al.* [2] have integrated a fiber bending sensor into a bed sheet to monitor human respiration during sleep. Besides, fiber bending/displacement sensors may operate as fiber cantilevers that are used for sensing force (weight) [3], liquid velocity and viscosity [4–6], vibration [6], and acceleration [7]. Many fiber bending sensors are also devoted to the R&D of robots [8,9]. Thanks to the flexibility and small size of fiber threads, the fiber bending sensors can be easily integrated with robot electro-mechanic modules and directly measure movements of a robot. Other areas where fiber bending sensors can find their applications include geological studies, structural health monitoring of architectures, and the car industry, to name a few.

According to their sensing mechanisms, fiber-optic bending sensors are generally categorized into two classes: intensity-based sensors and spectral-based sensors. Intensity-based sensors use either single-mode or multimode fibers; transmitted intensity through such fibers is then characterized as a function of the bending curvature [10,11]. Among the advantages of this type of bending sensors are low cost, ease of fabrication, and simple signal acquisition and

1559-128X/13/256344-06$15.00/0

processing since no spectral manipulations are required. However, the detection accuracy of the amplitude-based sensors is prone to errors due to intensity fluctuations of the light source and temperature drift. Moreover, in order to increase sensor sensitivity, it is preferable to strip as much as possible the cladding modes, which are excited by the bend. This is typically accomplished by coating the fiber cladding with an absorbing layer or by decorating the fiber cladding with scatterers such as scratches [10].

Spectral-based fiber-optic bending sensors can be implemented using fiber gratings that include both fiber Bragg gratings (FBGs) [12–14] and long-period gratings [15,16]. Bending of fiber gratings changes the pitch and refractive index (due to the photoelastic effect) of the gratings, thus shifting the resonant wavelengths. Compared to intensity-based sensors, fiber-grating bending sensors are generally more sensitive, and they allow multiplexing sensing of a number of other measurands such as temperature, strain, and refractive index [16]. The typical bending sensitivity of fiber-grating sensors is ~1–20 nm/m^{-1} [13–16]. Note that fiber-grating bending sensors normally require expensive characterization equipment such as spectrometers, while the bending resolution of fiber-grating-based sensors is limited by the spectrometer resolution.

The spectral-based sensing modality is also utilized by many in-line optical-fiber bending/displacement sensors that employ interferometric structures. In these sensors, the guided light is split into different components propagating along different (in-fiber) paths, or the guided light is coupled into different modes. Then the recombination of these components (or modes) would generate interference that is susceptible to bending of the fiber. By interrogating the shift of the interference fringes in the transmission spectrum, one can quantify fiber bending. Various fabrication techniques for the in-line fiber-optic interferometric sensors have been proposed. These include splicing a multimode fiber or photonic crystal fiber between two single-mode fibers [17–19], cascading two fiber tapers [20], splicing a photonic crystal fiber between two long-period gratings [21], and using multicore fibers [22,23]. The bending sensitivity of the in-line fiber-optic sensors can be as high as ~36 nm/m^{-1} [21]. We note that the resolution of these spectral-based in-line fiber sensors is frequently limited by the resolution of a spectrometer used in those setups. Some of the in-line fiber bending sensors may operate using intensity-based interrogation [4]; thus they are exempt from the use of costly spectral acquisition devices. However, most of the in-line optical-fiber sensors use complicated nonhomogeneous fiber-based structures that require significant fiber processing such as splicing, polishing, and microstructure machining.

In this paper, we demonstrate an amplitude-based fiber bending/displacement sensor that uses uniform plastic photonic bandgap Bragg fiber with one end coated with a silver layer. This type of fiber features a relatively low-loss plastic core surrounded by a multilayer dielectric reflector. This Bragg reflector is an efficient mode stripper for the wavelengths outside of the fiber bandgap. In fact, outside of the fiber bandgap, the core guided light penetrates strongly into the multilayer reflector region, which acts as a strong scatterer due to imperfections on the multilayer interfaces. Therefore, by interrogating the fiber at the wavelengths near the bandgap edge, high sensitivities to bending can be achieved. For comparison, we a test bending sensor based on a regular multimode fiber of similar outside diameter and length. We find that the Bragg-fiber-based sensor is more sensitive to bending as compared to sensors based on regular multimode fibers due to the presence of an efficient mode stripper in the form of a multilayer reflector. Besides, we show that the Bragg fiber bending sensor can be packaged into a compact sensor module by adopting the "MOSQUITO" sensor configuration detailed in [24].

In order to avoid confusion between FBGs and Bragg fibers, we note that in the FBGs, the grating is inscribed onto the fiber along the fiber length. This is done as a post-process after the fiber is fabricated. To inscribe the FBG, ultraviolet photolithography or femtosecond laser machining is generally utilized. This is an additional processing step that is used after fabrication of the optical fiber. As to the Bragg fiber used in our sensor, the Bragg reflector is distributed in the transverse direction of the fiber and is fabricated directly during the fiber drawing process [25]. By realizing a Bragg reflector directly during fiber fabrication, we avoid a costly postprocessing step of writing Bragg gratings into a traditional optical fiber. This is expected to significantly reduce the cost of the specialty optical fibers for bending sensing.

Besides, the Bragg fiber sensor in this work operates using a low-cost intensity-based detection strategy. At the edge of the photonic bandgap, the transverse Bragg reflector operates as an efficient mode stripper, which greatly improves the sensitivity of the optical fiber to bending. In contrast, the abovementioned FBG-based sensors and in-line fiber sensors normally operate using a costly spectral-based detection strategy that measures the shift of resonant wavelengths in response to the fiber bending. This requires using expensive optical spectrum analyzers, with the sensor sensitivity directly related to the resolution of the optical spectrum analyzer.

2. Experiments

The fiber used in this work is an all-polymer solid-core photonic bandgap Bragg fiber fabricated in our group [25]. In Fig. 1(a), we show a typical example of a Bragg fiber that features a polymethyl methacrylate (PMMA) core surrounded by a Bragg reflector consisting of an alternating PMMA/polystyrene (PS) multilayer (refractive index: 1.49/1.59). Such a multilayer is responsible for the appearance of a spectrally narrow transmission band (reflector

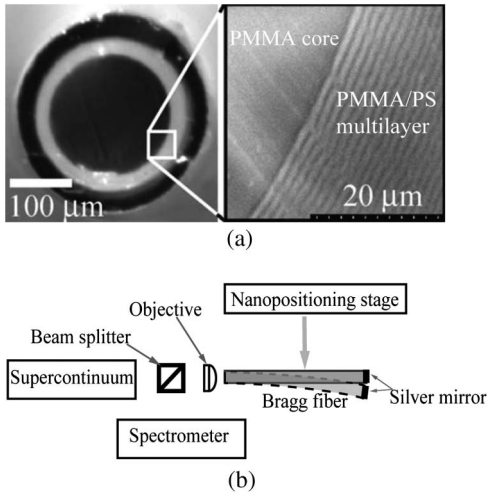

Fig. 1. (a) Cross section of a typical solid-core Bragg fiber. (b) Schematic of the Bragg fiber bending sensor.

bandgap) within which the light is strongly confined inside of the fiber core, with a minimal presence in the reflector region. For the wavelengths outside of the reflector bandgap, the light penetrates deeply into the multilayer region and suffers high propagation loss due to optical scattering on the imperfection of a multilayer. Experimentally, the typical propagation loss of a Bragg fiber is ~10 dB/m for the light inside the bandgap, and is ~60 dB/m for the light outside the bandgap. The position and width of the fiber bandgap are determined by the refractive indices of the fiber core and Bragg reflector as well as by the thicknesses of the individual layers in the Bragg reflector [26]. Additionally, one end of a Bragg fiber is wet-coated with a thin silver layer serving as a mirror [27].

In our experiment we use a 4-cm-long Bragg fiber with core/cladding diameters of 240/290 μm, featuring transmission losses at the bandgap center (~470 nm) ~20 dB/m and numerical aperture (NA) ~0.2–0.3 depending on the fiber length. At the bandgap edge (~500 nm), losses increase significantly, and so does the NA of a fiber that can be >0.8 for short fiber pieces. For comparison, we use a commercial 4-cm-long multimode plastic fiber with core/cladding diameters of 240/250 μm and NA ~0.5 for long fiber pieces. We note that direct comparison of the NAs of the two fibers is challenging (if not impossible), as the experimentally measured NA of short fiber pieces can be significantly different from that of the longer ones. Experimental measurements of NA of short fiber pieces are sensitive to the coupling conditions, as well as to the details of the intermodal scattering along the fiber length. This is further complicated by the observation that the NA of a Bragg fiber is highly sensitive to the operation frequency and can change from 0.2 at the bandgap center to more than 0.8 at the bandgap edge even for relatively long 20–30-cm-long fiber pieces. Therefore, for comparison, in our studies we have decided to use two different fiber types of the same core diameter and the same length, instead of fibers with the same NA, as would probably be more reasonable.

A schematic of the Bragg fiber bending sensor is presented in Fig. 1(b). The light from a supercontinuum source first passes through a beam splitter and is then coupled into the fiber by an objective. The light coupled into the fiber travels back and forth as it is reflected back by the silver mirror at the fiber end. The reflected light passes through an objective, and it is finally redirected by the beam splitter into a spectrometer for analysis. We note that a supercontinuum source and a grating-based spectrometer are only required to study the dependence of the bending sensor sensitivity on the wavelength of operation. Normally, they should be replaced with a laser diode and a power detector. Finally, a glass plate fixed on the nanopositioning stage is used to displace the fiber with increments of 50 μm to provide precisely measured displacements. The glass plate is positioned ~4 mm from the V groove.

In Fig. 2, we show a typical micrograph of a bent Bragg fiber. In order to extract the bend curvature, the fiber shape is fitted with a circular arc (3-point fitting). For larger displacements, the fiber shape starts to deviate from a simple circular arc, and consequently, error in the determination of the curvature increases with displacement. To estimate the

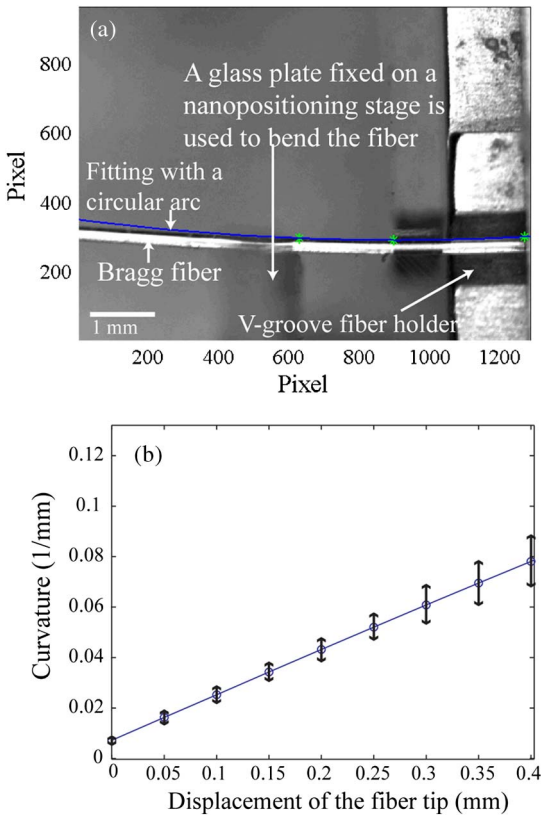

Fig. 2. (a) Fitting of the Bragg fiber shape with a circular arc. (b) Curvature of the Bragg fiber as a function of the displacements of the nanopositioning stage. The errors are estimated from the results of several alternative fittings.

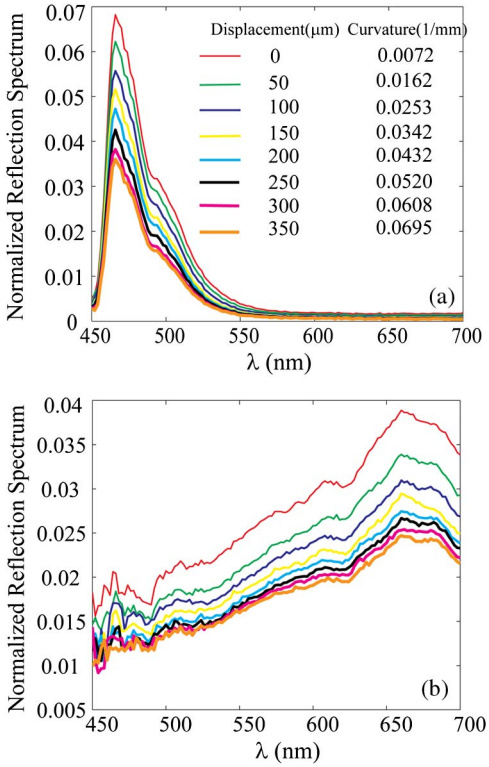

Fig. 3. Reflection spectra of (a) Bragg fiber and (b) regular multimode fiber for various values of the fiber curvature. The displacements of each fiber and the corresponding curvatures of the fitting arc are shown in the inset of (a).

error of the circular arc fitting, we perform a series of 3-point fittings by choosing different sets of fitting points on the fiber, and then find the maximum and minimum of the bending curvatures obtained. The reflection spectra of the Bragg fiber and the regular multimode fiber are presented in Fig. 3 for various values of the curvature.

From Fig. 3, it is clear that for both fibers, the intensity of the reflected light decreases strongly even for relatively large values of the bending radii, 2–10 cm. For the Bragg fiber, the bandgap center (the frequency of maximal transmission) remains fixed at ~470 nm, while the bandgap extends from 460 to 520 nm.

3. Discussion of Bending/Displacement Sensitivity

From the results shown in Fig. 3, we can now find the frequency dependence of the amplitude sensitivity of the two bending sensors. Thus, in Figs. 4(a) and 4(b), we plot the relative intensity difference $(\Delta I/I)$ caused by a 50 μm displacement and a 200 μm displacement of the fiber tip. We note that the amplitude sensitivity of the regular multimode fiber sensor is approximately constant in the whole spectral range, while the amplitude sensitivity of the Bragg fiber increases significantly when operating in the vicinity of a bandgap edge. In fact, at the edge or outside of the reflector bandgap, the Bragg-fiber-based sensor becomes more sensitive than the regular multimode-fiber-based sensor.

As explained earlier, in the vicinity of a reflector bandgap, the multilayer reflector of the Bragg fiber acts as an efficient mode stripper that allows scattering of the higher-order cladding modes excited by the bend. Unfortunately, we also have to note that in the bandgap vicinity, the propagation loss of the Bragg fibers becomes high, which leads to a significant signal-to-noise degradation for wavelength longer than 550 nm [see Figs. 4(a) and 4(b)]. Therefore, when choosing the optimal sensing wavelength at the bandgap edge, one faces a trade-off between the enhanced sensitivity and decreased signal-to-noise ratio. Besides, comparison between Figs. 4(a) and 4(b) also suggests that the Bragg fiber sensor becomes more sensitive than the regular multimode fiber sensor, regardless of the operation wavelength, when dealing with larger displacements. Thus, in Fig. 4(c), we present the relative change in the total transmitted intensity through the fiber as a function of the fiber displacement. Particularly, when the fiber tip is displaced by d, the relative change in the total fiber intensity δ is defined as

$$\delta(d) = \sum_{\lambda}[(I(\lambda,0) - I(\lambda,d)]\Big/\sum_{\lambda} I(\lambda,0), \qquad (1)$$

where $I(\lambda, 0)$ refers to the wavelength-sensitive output intensity of the fiber with no bending, $I(\lambda, d)$ is the output intensity of the fiber displaced by d, and λ is the wavelength. From Fig. 4(c), it is apparent that when the displacement of the fiber is larger than 150 μm, the Bragg fiber sensor becomes more sensitive than the multimode fiber sensor.

In order to estimate amplitude sensitivity S of the Bragg-fiber-based sensor, we use the following definition: $S(\lambda) = (\partial I(\lambda,\sigma)/\partial\sigma|_{\sigma=0})/I(\lambda,0)$, where σ can be either the displacement or the curvature of a fiber

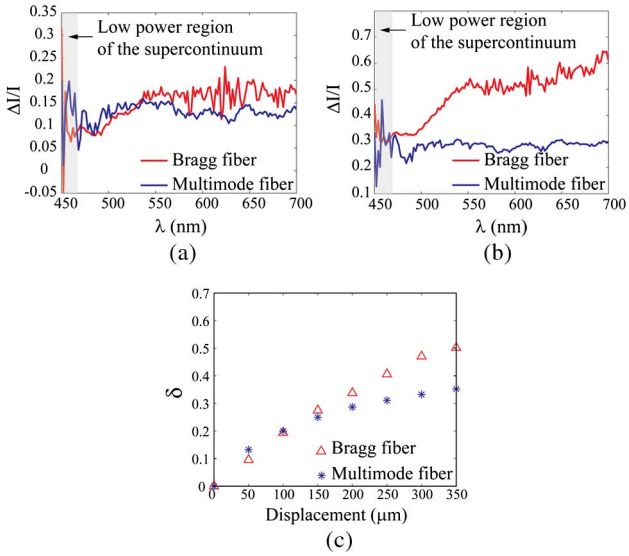

Fig. 4. Relative reflected intensity difference $\Delta I/I$ for a Bragg fiber sensor subjected to (a) 50 μm and (b) 200 μm displacements of the fiber tip. (c) Relative change in the total reflected intensity δ of the Bragg fiber as a function of the fiber tip displacement.

[28]. From the data in Fig. 4, we estimate that the sensitivity of the Bragg-fiber-based sensor at the bandgap edge (550 nm) is ~18.4 $(1/\text{mm})^{-1}$ for bending curvature sensing and is ~3.3 mm^{-1} for displacement sensing, while the corresponding sensitivities of the multimode fiber are ~15.5 $(1/\text{mm})^{-1}$ and ~2.8 mm^{-1}, respectively. The sensitivity of the Bragg-fiber-based bending sensor becomes significantly larger than that of standard multimode fibers when operating at longer wavelengths (550–600 nm), or for stronger displacements of the fiber tip (>100 μm). Assuming that 1% change in the amplitude of reflected light can be detected reliably, the bending and displacement detection limits of the Bragg fiber sensor are ~5×10^{-4} (1/mm) and ~3 μm, respectively. Currently, we are working with the SENSORICA group to integrate Bragg fibers into their "MOSQUITO" bending sensor platform [24]. In this configuration, the Bragg fiber is integrated with a small LED source, a micro-beam splitter, and a micro-photodiode detector, to result in a highly compact bending sensor.

Finally, we would like to discuss how thermal variations would affect the performance of the Bragg fiber bending sensor. We first note that as the glass transition temperature (T_g) of PS and PMMA is in the range of 75°C–110°C [29,30], the Bragg fiber sensor cannot be used in high-temperature environments. Below T_g, an increase in temperature would lead to both thermal expansion and refractive-index changes of fiber materials, thus resulting in spectral shifts and shape change of the Bragg fiber bandgap. In order to evaluate the effects of temperature change on the fiber transmission spectrum, we, therefore, perform a transfer matrix method (TMM)-based simulation [31] to calculate the normalized transmission spectra of the fundamental HE_{11} mode in an 8-cm-long Bragg fiber. The temperature-dependent refractive index of PMMA and PS can be found in [29,30]. The linear thermal-expansion coefficient is 7×10^{-5} m/m · °C for PMMA [32] and 9×10^{-5} m/m · °C for PS [33]. The thicknesses of individual layers in the Bragg reflector, measured from the microscopic graphs, are 240 nm for PMMA and 270 nm for PS. The absorption coefficients of the fiber materials are measured experimentally. The simulated transmission spectra of the Bragg fiber at different temperatures are shown in Fig. 5(a). For simplicity, we only show results for the fundamental HE_{11} mode of a fiber into which most of the power (>90%) is coupled at the fiber input end.

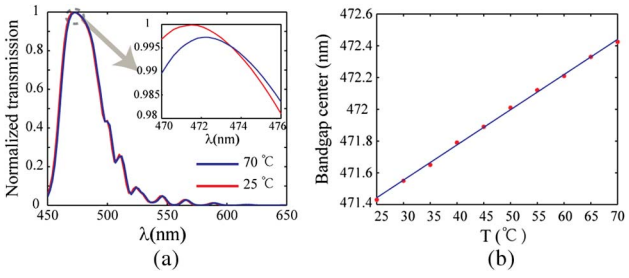

Fig. 5. (a) Simulated transmission spectra of the fundamental HE_{11} mode of the Bragg fiber used in experiments at 25°C and 70°C. (b) Spectral position of the bandgap center at various operation temperatures.

Figure 5(a) suggests that the Bragg fiber bandgap shows a red shift as the temperature increases. In Fig. 5(b), we observe that this spectral shift has a linear dependence on the surrounding temperature and that a 1°C increment in temperature would shift the bandgap position by ~22 pm. We note that in the middle of a bandgap, the effect of the temperature fluctuations on the transmission amplitude is minimal. Thus, in the whole 25–70°C range, the intensity change at the bandgap center is less than 1%. However, intensity variations at the bandgap edge can be more pronounced. From our simulations, we estimate the amplitude sensitivity to temperature variations to be ~1×10^{-4}/°C at the bandgap center, and ~2.0×10^{-3}/°C at the bandgap edge (around 500 nm). To put these numbers into a perspective, while operating at the bandgap edge (in order to increase the sensor sensitivity), the sensor stability range of temperatures is estimated to be 5°C, which would guarantee power fluctuations less than 1%.

4. Conclusions

In conclusion, we demonstrate a bending/displacement fiber-optic sensor based on the all-polymer photonic bandgap Bragg fibers. We find that when operated at the edge of a fiber bandgap, the Bragg-fiber-based sensor is more sensitive to bending as compared to the sensor that uses a regular multimode fiber of comparable diameter. The sensitivity of the Bragg-fiber-based bending sensor can become significantly larger than that of a standard multimode-fiber-based sensor when operating at a wavelength outside of the bandgap, or for stronger displacements of the fiber tip (>100 μm). This is due to action of an efficient mode stripper in the form of a multilayer reflector that is present in the Bragg fiber. Displacements as small as 3 μm and bending radii as large as 1 m can be detected with the Bragg-fiber-based sensor. Finally, we also study how temperature variations would affect the performance of the Bragg-fiber-based bending sensor and estimate that temperature variations of 5°C result in power variation of 1%, which has to be taken into account when operating at the limit of sensor sensitivity.

We thank Prof. Takaaki Ishigure from Keio University for hosting Prof. M. Skorobogatiy during his JSPS-sponsored research stay in Japan. During this stay, we performed extensive characterization of plastic Bragg fibers, which we used in this work.

References

1. http://www.sensorica.co/home/projects/mosquito/philippe-s-project/announcements---philippe-poject/themosquitomeasuresmusclecontraction.
2. S. Mitachi, D. Shiroishi, and M. Nakagawa, "Development of a sleep apnea syndrome sensor using optical fibers," in

Proceedings of the 20th Annual Meeting of the IEEE Lasers and Electro-Optics Society (IEEE, 2007), pp. 294–295.
3. A. Kulkarni, J. Na, Y. Kim, and T. Kim, "The plastic optical fiber cantilever beam as a force sensor," Microw. Opt. Technol. Lett. **51**, 1020–1023 (2009).
4. L. Yuan, J. Yang, and Z. Liu, "A compact fiber-optic flow velocity sensor based on a twin-core fiber Michelson interferometer," IEEE Sens. J. **8**, 1114–1117 (2008).
5. P. Liu and Q. Chen, "Fiber Bragg grating cantilever sensor system for liquid flow monitoring with temperature compensation," Proc. SPIE **7753**, 77538L (2011).
6. P.-Y. Ju, C.-H. Tsai, L.-M. Fu, and C.-H. Lin, "Microfluidic flow meter and viscometer utilizing flow-induced vibration on an optical fiber cantilever," in *Proceedings of the 16th International Solid-State Sensors, Actuators and Microsystems Conference*, Beijing, China (IEEE, 2011), pp. 1428–1431.
7. M. Morante, A. Cobo, J. M. Lopez-Higue, and M. Lopez-Amo, "New approach using a bare fiber optic cantilever beam as a low-frequency acceleration measuring element," Opt. Eng. **35**, 1700–1706 (1996).
8. M. H. Khorasani, C. Menon, M. V. Sarunic, M. Gharehbaghi, and Y. Li, "Towards a miniaturized embeddable sensor for multi-DOF robotic system," in *Proceedings of the 2nd IEEE/RAS & EMBS International Conference on Biomedical Robotics and Biomechatronics*, Scottsdale, Arizona (IEEE, 2008), pp. 664–669.
9. D.-Z. Tan, Q.-M. Wang, R.-H. Song, X. Vao, and Y.-H. Gu, "Optical fiber based slide tactile sensor for underwater robots," J. Marine Sci. Appl. **7**, 122–126 (2008).
10. Y. Fu, H. Di, and R. Liu, "Light intensity modulation fiber-optic sensor for curvature measurement," Opt. Laser Technol. **42**, 594–599 (2010).
11. K. S. C. Kuang, W. J. Cantwell, and P. J. Scully, "An evaluation of a novel plastic optical fiber sensor for axial strain and bend measurements," Meas. Sci. Technol. **13**, 1523–1534 (2002).
12. X. Chen, C. Zhang, D. J. Webb, K. Kalli, and G. D. Peng, "Highly sensitive bend sensor based on Bragg grating in eccentric core fiber," IEEE Photon. Technol. Lett. **22**, 850–852 (2010).
13. Y.-S. Yu, Z.-Y. Zhao, Z.-C. Zhuo, W. Zheng, Y. Qian, and Y.-S. Zhu, "Bend sensor using an embedded etched fiber Bragg grating," Microw. Opt. Technol. Lett. **43**, 414–417 (2004).
14. Y.-G. Han, "Directional bending sensor with temperature insensitivity using a sampled chirped fiber Bragg grating," J. Appl. Phys. **105**, 063103 (2009).
15. H. J. Patrick and S. T. Vohra, "Long period fiber grating for structural bend sensing," Electron. Lett. **34**, 1773–1775 (1998).
16. S. W. James and R. P. Tatam, "Optical fiber long-period grating sensors: characteristics and application," Meas. Sci. Technol. **14**, R49–R61 (2003).
17. Y. Gong, T. Zhao, J. Rao, and Y. Wu, "All-fiber curvature sensor based on multimode interference," IEEE Photon. Technol. Lett. **23**, 679–681 (2011).
18. M. Deng, C.-P. Tang, T. Zhu, and Y.-J. Rao, "Highly sensitive bend sensor based on Mach–Zehnder interferometer using photonic crystal fiber," Opt. Commun. **284**, 2849–2853 (2011).
19. D. Chen, F. Xu, G. Hu, L. Chen, and B. Peng, "Fiber bending sensor based on a two mode fiber," Microw. Opt. Technol. Lett. **54**, 1047–1049 (2012).
20. D. M. Hernandez, A. Martinez-Rio, I. Torres-Gomez, and G. Salceda-Delgado, "Compact optical fiber curvature sensor based on concatenating two tapers," Opt. Lett. **36**, 4380–4382 (2011).
21. W. Shi, Y. L. Lee, B. Yu, Y. Noh, and T. J. Ahn, "Highly sensitive strain and bending sensor based on in-line fiber Mach–Zehnder interferometer in solid core large mode area photonic crystal fiber," Opt. Commun. **283**, 2097–2101 (2010).
22. R. M. Silva, M. S. Ferreira, J. Kobelke, K. Schuster, and O. Frazao, "Simultaneous measurement of curvature and strain using a suspended multicore fiber," Opt. Lett. **36**, 3939–3941 (2011).
23. J. Yang, L. Yuan, X. Zu, Y. Zhang, and B. Liu, "Twin-core fiber white light interferometric bending sensor," Proc. SPIE **7004**, 70040Y (2008).
24. http://www.sensorica.co/home/projects/mosquito.
25. A. Dupuis, N. Guo, B. Gauvreau, A. Hassani, E. Pone, F. Boismenu, and M. Skorobogatiy, "Guiding in the visible with "colorful" solid-core Bragg fibers," Opt. Lett. **32**, 2882–2884 (2007).
26. H. Qu, B. Ung, N. Guo, and M. Skorobogatiy, "Photonic bandgap fiber bundle spectrometer," Appl. Opt. **49**, 4791–4800 (2010).
27. http://www.sensorica.co/home/projects/optical-fiber-coating/announcements---fiber-coating/wetsilvercoatingcanbeautomated.
28. M. Skorobogatiy, "Microstructured and photonic bandgap fibers for applications in the resonant bio- and chemical sensors," J. Sens. **2009**, 524237 (2009).
29. S. Karuse and Z.-H. Lu, "Refractive index-temperature measurements on anionically polymerized polystyrene," J. Polym. Sci. **19**, 1925–1928 (1981).
30. H. Lin, D. E. Day, K. D. Weaver, and J. O. Stoffer, "Temperature and wavelength dependent transmission of optically transparent glass fiber poly(methyl methacrylate) composites," J. Mater. Sci. **29**, 5193–5198 (1994).
31. S. G. Johnson, M. Ibanescu, M. Skorobogatiy, O. Weiseberg, T. D. Engeness, M. Soljacic, S. A. Jacobs, J. D. Joannopoulos, and Y. Fink, "Low-loss asymptotically single-mode propagation in large core OmniGuide fibers," Opt. Express **9**, 748–779 (2001).
32. http://www.spyroplastics.com/products/pdf/spyrex_typical_properties.pdf.
33. W. D. Callister and D. G. Rethwisch, *Fundamentals of Materials Science and Engineering: An Integrated Approach*, 3rd ed. (Wiley, 2008), pp. 708–709.